Dynamics of resonances and uncertainty of parameters in a ring-like system

Alessandra Celletti
celletti@mat.uniroma2.it

University of Rome Tor Vergata

Irene De Blasi
University of Turin

Sara Di Ruzza
University of Palermo

Article

Keywords: Rings, Small bodies, Resonances, Libration, Stability

Posted Date: July 15th, 2026

DOI: https://doi.org/10.21203/rs.3.rs-7693965/v2

Additional Declarations: The authors declare no competing interests.

Dynamics of resonances and uncertainty of parameters in a ring-like system

Alessandra Celletti[1,+,*], **Irene De Blasi**[2,+], **and Sara Di Ruzza**[3,+]

[1]Department of Mathematics, University of Roma Tor Vergata, Via della Ricerca Scientifica 1, 00133 Roma (Italy)
[2]Department of Mathematics, University of Torino, via Carlo Alberto 10, Torino,(Italy)
[3]DMI, University of Palermo, Via Archirafi, 34, 90123 Palermo, (Italy)
[*]celletti@mat.uniroma2.it

ABSTRACT

The discovery of rings surrounding small celestial bodies has been a recent advancement made possible through ground-based stellar occultations. Notably, dense and narrow rings have been identified encircling the dwarf planet (136108) Haumea, the Centaur (10199) Chariklo, the trans-Neptunian object (50000) Quaoar. These rings are observed in a specific dynamical configuration known as the 1:3 resonance, which correlates the orbit of a ring particle with the rotation of the central body, wherein their periods maintain a 1/3 ratio. In this study, we provide dynamical arguments in strong support to the preference shown by the small bodies for the 1:3 resonance over alternative resonances. Our findings are exclusively based on the consideration of the potential of the central body, without invoking other effects, such as those potentially induced by satellites of the small bodies.

KEYWORDS
Rings, Small bodies, Resonances, Libration, Stability

1 Introduction

We consider a small body rotating about its spin-axis and surrounded by one or more rings, consisting of particles of negligible size. Consequently, two principal periods are identified: the rotational period of the small body and the orbital period of a particle in the ring. A spin-orbit resonance of order $m:n$ (with m, n integers) occurs when the rotational and the orbital periods stay in the ratio $m:n$. We notice that later we will introduce Lindblad resonances (which are more appropriate in rings dynamics), that include also the rate of variation of the argument of periastrum.

Within the small bodies of the Solar system, Haumea[1–3] possesses a ring with approximate width of 70 km. Furthermore, the presence of two narrow rings[4–7] around Chariklo, designated 2013C1R and 2013C2R, was documented with widths approximately 7 and 3 km. Also Quaoar shows two rings[8–10], Q1R with a width between 5 and 300 km and Q2R with a width of about 10 km. It is noteworthy that the rings around Chariklo, Haumea and Q1R for Quaoar are located close to a spin-orbit resonance[11] of order 1:3. Therefore, it appears that the ring systems surrounding these small celestial bodies preferentially select a specific resonance while excluding other resonances, such as the corotation, also named 1:1 resonance (wherein the ring particles orbit with the same period as the rotational period of the central body) or resonances of different orders, e.g. the 1:2, 2:3, and 2:5 resonances. The phenomenon of selecting specific resonances is well-established in Celestial Mechanics. A remarkable example is given by the main belt asteroids, some of them being observed in mean motion resonances, defined as commensurabilities between the orbital period of the asteroid and that of Jupiter. Although asteroids can be observed at mean motion resonances of order 1:1 and 2:3, the resonances of order 1:2, 1:3, 1:4, 2:5, and 3:7, commonly referred to as "Kirkwood gaps", have been determined to be devoid of asteroids[12]. Numerous studies have been conducted to explain the mechanisms responsible for the depletion or selection of these resonances[13–19]. In this study, we propose potential explanations for the 1:3 resonance selection by the rings' particles encircling the small celestial bodies Haumea, Chariklo, Quaoar. The present analysis exclusively considers dynamical effects and examines whether a model that incorporates solely the potential of the central body accounts for the selection of the 1:3 resonance, independently of ancillary effects such as the gravitational influence of satellites orbiting the small body.

To describe the gravitational potential of the small object, we employ a model derived by representing the central body as a triaxial homogeneous ellipsoid with semi-axes $a > b > c$, rotating about the smallest axis[13,20–22]. We introduce two shape parameters: elongation and oblateness, defined as

$$\mathscr{E} = \frac{a^2-b^2}{2R^2}\ , \qquad \Omega = \frac{a^2+b^2-2c^2}{4R^2}\ , \tag{1}$$

where R is the *reference length:*

$$R = \left(\frac{3}{a^{-2} + b^{-2} + c^{-2}} \right)^{\frac{1}{2}} . \tag{2}$$

Furthermore, we consider that the ring's particle moves on the equatorial plane. The motion of the particle is conveniently described using Hamiltonian formalism expressed in terms of the epicyclic variables, which comprehensively encapsulate the problem's dynamics and offer the benefit of representing action-angle variables pertinent to the Hamiltonian (see "Methods"). An alternative model is described by the so-called *topographic feature*[23,24], comprising a sphere with an attached mass anomaly situated on the surface of the body along the equatorial plane.

In this work, we study the dynamics of the main resonances under the ellipsoidal model, although we analyzed also the topographic features which yield results analogous to the ellipsoidal model. The goal is to provide dynamical evidence to substantiate that the particles within the rings surrounding Haumea, Chariklo, Quaoar preferentially select the 1:3 resonance, while disregarding alternative resonances. Our primary objective is to address the following inquiries: (Q1) Is the 1:3 resonance dynamically more robust than other resonances? (Q2) Is the potential generated by the central body adequate to account for the differences among the resonances? (Q3) Do the shape parameters play a role in the dynamical behavior of the resonances?

The answers to these questions rely on a specific procedure where, for a given resonance, the Hamiltonian is systematically transformed as follows: (1) introduce variables tailored to the resonance, (2) expand (up to suitable orders) the Hamiltonian function in Taylor series in the actions and Fourier series in the angles, (3) average the Hamiltonian and retain only the terms of the expansion that correspond to the resonant combinations of the angles. Using this Hamiltonian, we undertake an investigation into the dynamical effects of the (strong) non-axisymmetric gravitational field of a triaxial ellipsoid by examining and weaving the following dynamical aspects characterizing each resonance: the amplitude of the libration region surrounding the stable equilibria, the stability time of the orbital elements, the dependence of the results on the shape parameters, the linear stability of the equilibrium points, the occurrence of bifurcations as the eccentricity is varied.

The main parameters are reported in Table 1 for Haumea[24], Chariklo[24,25] and Quaoar[26]. The reference radius R is computed through Eq. (2). We also give the Roche limit for Haumea[1], Chariklo[27], Quaoar[9]. The distances from the center of the small body of the 1:1, 1:2, 1:3, 2:3 resonances are obtained using the relation defining a Lindblad resonance as in Eq. (3) (defined in Section 2), which can be solved for the radius.

	Haumea	Chariklo	Quaoar
mass (kg)	$4.006 \cdot 10^{21}$	$6.3 \cdot 10^{18}$	$1.2 \cdot 10^{21}$
rotation period T_P (h)	3.915341	7.004	17.6788 (or 8.8494)
semi axes a, b, c (km)	1161,852,513	138,118.68,105.62	643.05,540.38,465.85
reference radius R (km)	712	118	536
Roche limit (km)	4400	< 300	1780
Observed ring radii (km)	2287	390 and 405	4157 and 2520
1:1 ring (km)	1189.80	192.167	2024.58
1:2 ring (km)	1740.26	300.212	3203
1:3 ring (km)	2278.02	392.981	4196.06
2:3 ring (km)	1450.92	248.546	2645.73

Table 1. Parameters of Haumea, Chariklo and Quaoar.

2 RESULTS

Set-up of the model

The potential generated by the ellipsoid at a distance r from its barycenter is a function $V = V(r, \theta)$, where $\theta = L - \Omega_P t$ with L the true longitude of the particle in an inertial frame and Ω_P the rotational velocity of the small body. The synodic and epicyclic frequencies are introduced as $\nu = n - \Omega_P$ and $\kappa = n - \dot{\omega}$ with n the mean motion and $\dot{\omega}$ the rate of variation of the argument of periastrum. A Lindblad resonance of order $m : (m - j)$, for m, j integers, occurs when

$$j\kappa(r) = m\nu(r) ; \tag{3}$$

a special case is given by the corotation resonance corresponding to $j = 0$. For a given resonance, let r_* be the corresponding radius, which can be computed through (3). Let $\rho = r - r_*$ be the distance from the resonance and p_ρ the corresponding momentum; let $I = p_\theta - p_*$ be the displacement from the resonant value $p_* = n(r_*)r_*^2$ of the angular momentum p_θ conjugated to θ. The epicyclic variables (J,φ) are defined through the relations

$$\rho = \sqrt{\frac{2J}{|\kappa(r_*)|}}\ \sin\varphi\ , \qquad p_\rho = \sqrt{2|\kappa(r_*)|J}\ \cos\varphi\ .$$

The 2D Hamiltonian of the ring's dynamics is given by

$$\mathscr{H}(J,I,\varphi,\theta) = |\kappa(r_*)|J + \nu(r_*)I + F_s(J,I,\varphi) + F_{ns}(J,\varphi,\theta)\ ,$$

where F_s and F_{ns} denote, respectively, the axisymmetrical and non-axisymmetrical parts of the potential (see "Methods"). For a specific resonance, the Hamiltonian is expanded in Taylor series of the actions and Fourier series of the angles; the expansions are truncated to a finite order and only the resonant terms are retained. Denote by (G,L,ψ,μ) the resonant set of coordinates with $\psi = -m\theta + j\varphi$ the resonant angle for a resonance of order $m:(m-j)$. The variable μ is cyclic, hence $L = L_0$ is a constant of motion; we are thus led to a 1D Hamiltonian that we can write to second order as

$$\mathscr{H}(G,\psi;L_0) = \alpha_1(L_0)G + \alpha_2(L_0)G^2 + \beta_1(G;L_0)\ \mathrm{cs}(\psi) + \beta_2(G;L_0)\ \mathrm{cs}(2\psi)\ , \tag{4}$$

where, according to the chosen resonance, cs stands for cosine or sine and α_i, β_i are polynomials. In the next sections, the Hamiltonian (4) is used to explore the dynamics of the 1:1, 1:2, 1:3, 2:3 resonances, and the associated stable and unstable equilibria.

Amplitude of libration around the resonances

A measure of the stability of the resonances is given by the amplitude of the libration region around the stable equilibrium point associated to the resonance. To estimate the amplitude of libration, we use Hamilton's equations associated to (4) from which we compute the stable equilibrium (ψ_0, G_0) and estimate the amplitude of the surrounding libration island in the (ψ,G)-plane as the maximum distance ΔG of the two separatrices originated from the unstable point. The results are summarized in Figure 1 in terms of the distance $\Delta G = G_{max} - G_{min}$ with G_{max}, G_{min} the values corresponding to the upper and lower separatrix at $\psi = \psi_0$. The quantity ΔG is plotted versus the eccentricity from 0 to 0.3, which represents a reasonably high value for the eccentricity.

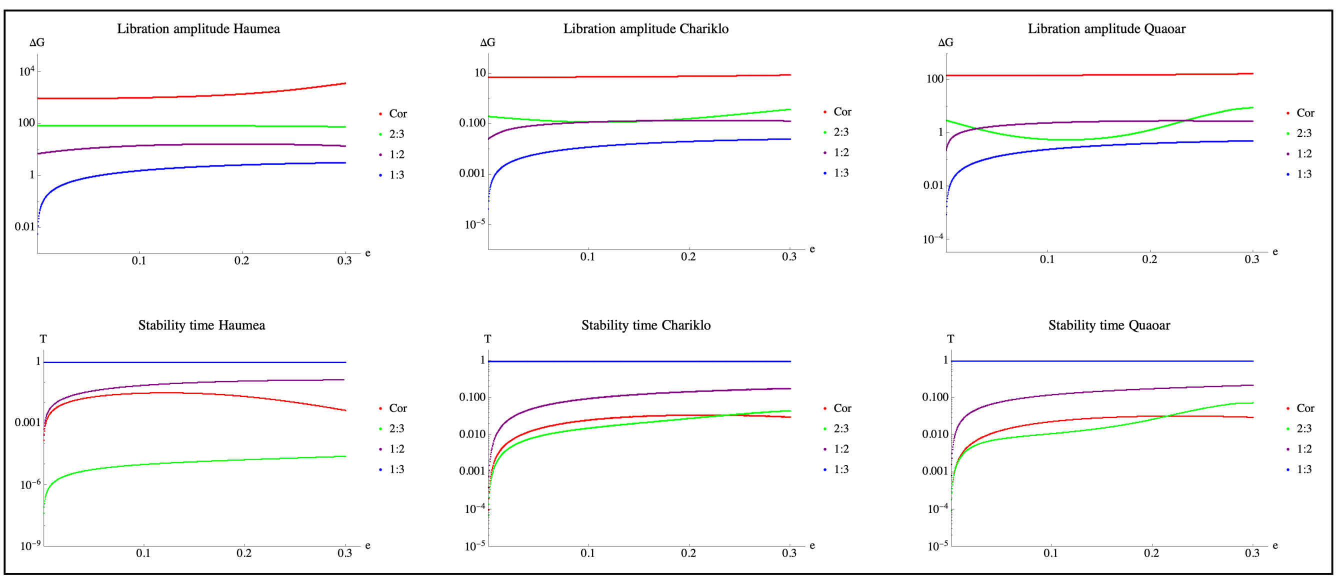

Figure 1. Amplitudes (top panels) of libration of the action variable G (in rad km^2/s) and ratio of the stability time (bottom panels) of the action variable G for corotation, 2:3, 1:2, 1:3 resonances versus the stability time of 1:3 resonance as function of the eccentricity, for the three bodies Haumea (left), Chariklo (middle), Quaoar (right).

Figure 1 (top panels) shows that the smallest amplitude of libration is always associated with the 1:3 resonance, thereby suggesting that this resonance is the most regular. In fact, as a consequence of the smaller amplitude, it is less likely that the 1:3 resonance overlaps with other resonances (which is a well-known source of chaos); furthermore, the phase space around the 1:3 resonance is chiefly occupied by invariant rotational KAM tori, that provide a strong stability property in the sense of confinement in phase space[28]. These observations are of substantial significance, as they give a first support to the claim that the 1:3 resonance is the most advantageous from a dynamical perspective.

Stability time

A crucial information characterizing each resonance is represented by the estimate of the stability time of the action variable: we compute the time for the action to reach a given excursion from its initial value[29]. This information is obtained from Hamilton's equation associated to (4):

$$\dot{G} = -\frac{\partial \mathscr{H}}{\partial \psi} \ . \tag{5}$$

One can bound the excursion of G up to a time T by using the mean value theorem:

$$|G(T) - G(0)| \leq |\dot{G}| \ T \ . \tag{6}$$

Fixing a maximum excursion ΔG, and using (5), (6), one gets the stability time

$$T = \frac{\Delta G}{\left\| \frac{\partial \mathscr{H}}{\partial \psi} \right\|} \ , \tag{7}$$

where the norm in (7) is computed by taking the supremum over $\psi \in [0, 2\pi)$ and G within the libration island, say $G \in [G_{min}, G_{max}]$. The stability times computed by Eq. (7) are presented in Figure 1 (bottom panels). We are aware that such stability times are irrelevant from the astronomical point of view; however, these values are obtained implementing just a first order estimate. The stability times can be improved by implementing higher order normal forms as well as effective stability estimates á la Nekhoroshev[30,31]. In Figure 1 we plot the stability times computed for the 1:1, 2:3, 1:2 resonances normalized with respect to the values, at each eccentricity, of the stability time of the 1:3 resonance (hence, the stability time of the 1:3 resonance is a straight line with unitary value). The results show that the highest stability time always corresponds to the 1:3 resonance.

Dependence of the amplitude on the shape parameters

Small bodies are often characterized by an irregular shape. By assuming a model in which the small body is an ellipsoid, the parameters that quantify the shape are elongation and oblateness (Eq. (1)). Additionally, significant parameters that may influence the position and stability of the resonances include the mass M_P and the rotational period T_P.

We study the stability of the equilibria as a function of the shape parameters, analysing different situations: in Table 2, we propose four different sets of semi-axes and/or periods for each body, taking into account the experimental uncertainties associated with the dimensions of the small celestial bodies. In particular, the four cases for Haumea have been chosen within the uncertainties on the semi-axes[1], as well as the four cases for Chariklo[25]. As for Quaoar, we chose two cases within the predicted uncertainties on the semi-axes[26] and both of them are analyzed with two hypothesized periods[9]. For all three bodies, case 1 corresponds to the central values of the semi-axes, and for Quaoar to the preferred period.

Figure 2 shows the amplitudes of libration of Haumea, Chariklo and Quaoar, given as a function of $\mathscr{E}$, Ω (as defined in Eqs. (1)) for two values of the eccentricities, namely $e = 0.001$ and $e = 0.3$ for the 1:1, 1:2, 1:3 resonances. The color scale gives the amplitude in rad km^2/s. In all plots, $\mathscr{E} \times \Omega \in [0, 1]^2$, thus covering all physically relevant cases, including those listed in Table 2.

In the top left panel, representing Haumea, the black point has coordinates $\mathscr{E} = 0.615, \Omega = 0.765$, which are, respectively, the elongation and oblateness of Haumea 1, Table 2. We observe that the amplitude increases with eccentricity ($e = 0.001$, $e = 0.3$, top and bottom plots, respectively) and elongation (which is represented on the horizontal axis), while it is less sensitive to variations in oblateness (shown on the vertical axis), except for the corotation, where the dynamics of the particle is more influenced by oblateness due to the vicinity of the orbit to the ellipsoid. The smallest amplitude occurs for the 1:3 resonance, whatever the values of $\mathscr{E}$ and Ω are. A behavior similar to Haumea is observed for Chariklo and Quaoar. In the top right panel, representing Chariklo, the black point has coordinates $\mathscr{E} = 0.175, \Omega = 0.191$, which are, respectively, the elongation and oblateness of Chariklo 1, Table 2. The behavior arising from the parameter dependence is analogous to that observed for Haumea. Finally, Quaoar is shown in the bottom panel. The black point has coordinates $\mathscr{E} = 0.211, \Omega = 0.236$, which are, respectively, the elongation and oblateness of Quaoar 1, Table 2. Also in this case, a very strong dependence on elongation (horizontal axis) is observed, while the dependence on orbital eccentricity and oblateness is negligible. This is probably due to the fact that the resonant particles are located far from the central body, since the resonance radii (even that of the 1:1 resonance) are much larger than the semi-axes as a consequence of Quaoar's slow rotation rate.

	a (km)	b (km)	c (km)	T_P (h)	$\mathscr{E}$	Ω
Haumea 1	1161	852	513	3.915341	0.615	0.765
Haumea 2	1191	856	529	3.915341	0.645	0.749
Haumea 3	1131	848	497	3.915341	0.581	0.781
Haumea 4	1191	852	497	3.915341	0.709	0.844
Chariklo 1	138	118.68	105.62	7.004	0.175	0.191
Chariklo 2	154	133	123	7.004	0.165	0.153
Chariklo 3	122	100	86	7.004	0.244	0.252
Chariklo 4	154	116	86	7.004	0.432	0.471
Quaoar 1	643.05	540.38	465.85	17.6788	0.211	0.236
Quaoar 2	666.65	560.21	482.94	17.6788	0.211	0.236
Quaoar 3	643.05	540.38	465.85	8.8494	0.211	0.236
Quaoar 4	666.65	560.21	482.94	8.8494	0.211	0.236

Table 2. Four cases for Haumea, Chariklo, Quaoar.

In all three bodies, it is clearly evident that the 1:3 resonance exhibits much smaller amplitudes compared to the other resonances, regardless of the parameters.

Bifurcation diagrams

The linear stability of the equilibria is studied through the linearization of the equations of motion and the computation of the corresponding eigenvalues at the equilibrium. When the eigenvalues are purely imaginary, the equilibrium is of center type, hence stable; conversely, when the eigenvalues possess a non-zero real part, the equilibrium is a saddle, consequently unstable. The eigenvalues of the linear system are determined as a function of the eccentricity within 0 and 0.3.

We start by analyzing the four cases of Haumea in Table 2. For the 1:1 resonance, the bifurcation diagram (see Figure 3, panel A on the left), shows that the equilibrium point $\psi = 0$ is a center and $\psi = \pi/2$ is a saddle; at $\psi = 1.183$, a saddle-node bifurcation arises at $e_{cor} = 0.247$ for Haumea 4 and for $e > e_{cor}$ for the other cases; for Haumea 3 (the less elongated case) it appears for $e > 0.3$, thus it is not displayed in the figure. These results are corroborated by the phase portrait of Haumea 1 computed for $e = 0.3$ (panel A on the right). Figure 3 (panel A) provides also the amplitude of libration for all four cases.

A different situation occurs for the 1:2 resonance (see Figure 3, panel B on the left) for which the equilibrium $\psi = \pi$ shows a double pitchfork bifurcation: it is of center type for small eccentricities; its linear stability changes at $\underline{e}_{12} = 0.118$ for Haumea 4 (and nearby values for the other cases) becoming of saddle type and returning to center type at $\overline{e}_{12} = 0.266$ (for Haumea 4). For $e < \underline{e}_{12}$ and $e > \overline{e}_{12}$ two secondary unstable solutions arise from the pitchfork bifurcation. The phase portrait in panel B (on the right) shows the presence of such equilibria for Haumea 1 at $e = 0.3$.

The 1:3 resonance exhibits the noteworthy characteristic of maintaining stability without experiencing bifurcations as confirmed by the phase portrait around the 1:3 resonance, showing no change in the stability of the equilibria; the only difference as the eccentricity or the ellipsoid dimensions vary is a slight change in the sizes of the amplitudes of libration (see Figure 3, panel C on the left).

The same methodology was applied to the cases of Table 2 for Chariklo and Quaoar (see Figure 4) yielding results that confirm that only the 1:3 resonance remains stable with the eccentricity. For both Chariklo and Quaoar, the 1:1 resonance does not show bifurcations, though it has a larger amplitude in comparison to the 1:3 resonance, as shown in Figure 1 (center and right panels, respectively) while the 1:2 resonance experiences the same pitchfork bifurcations as for Haumea. In Figure 4, panel A, top left, we present the bifurcation diagram for the four cases of Chariklo. The diagram shows that the pitchfork bifurcation occurs at very small values of the eccentricity, indicating enhanced instability near $e = 0$ in the 1:2 resonance. In the same panel, on the right, the two phase portraits at $e = 0.001$ and $e = 0.3$ illustrate the change in stability of the equilibrium point at $\psi = \pi$, as well as the presence or absence of unstable secondary equilibria at different eccentricities. The dynamics of the 1:2 resonance for Quaoar is similar to that of Haumea and Chariklo with amplitudes as in Figure 1 (right panels). In Figure 4, panel B, we show the 1:3 resonance for Quaoar, emphasizing the consistent stability behavior of its equilibria. Notice also how the change in period between Quaoar 1, 2 and Quaoar 3, 4 has a relevant effect on the amplitudes (panel B, on the left); however, it does not alter the fact that the 1:3 resonance remains the preferred one.

Finally, the 2:3 resonances is analyzed. As shown in Figure 1, it has large amplitudes and short stability times, but its main feature is to have many stability regimes depending on the values of the parameters and the eccentricity as represented in Figure 5. Haumea and Chariklo present phase portraits which are completely different from each others, while Quaoar undergoes a saddle-node bifurcation as the eccentricity varies. The phase portrait of Haumea 1, for $e = 0.3$, presents one

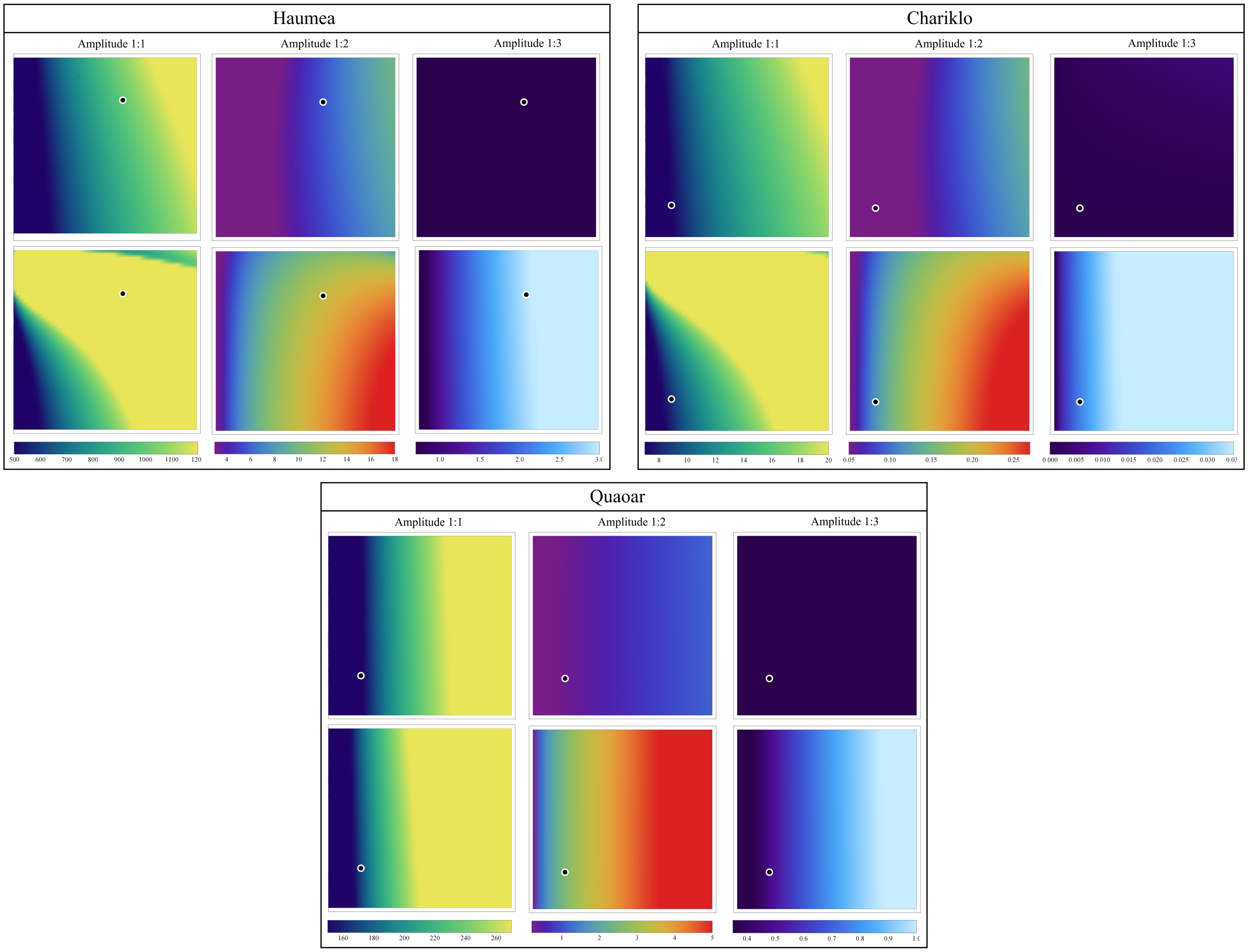

Figure 2. Dependence of amplitude on the shape parameters. Top left, Haumea; top right, Chariklo; bottom, Quaoar. The amplitude of libration (in rad km^2/s) of the action G is given as a function of the elongation parameter $\mathscr{E}$ (on the x-axis) and oblateness parameter Ω (on the y-axis) for 1:1, 1:2 and 1:3 resonances for two values of the eccentricity, $e = 0.001$ and $e = 0.3$, respectively, on top and bottom plots of each panel.

saddle point in $\psi = \pi/2$ and two secondary equilibria of center type with $\psi \in (0, \pi/2)$ and $\psi \in (\pi/2, \pi)$. Chariklo 1 has only one stable equilibrium point in $\psi = 3\pi/2$. Quaoar 1 experiences a saddle-node bifurcation at $e_{23} = 0.27$: for small values of the eccentricity it has only a stable equilibrium point in $\psi = 3\pi/2$ as plotted in the bottom left panel for $e = 0.015$; at $e = e_{23}$, in $\psi = \pi/2$ two new equilibria arise (one of center, the other of saddle type), as it is shown in the bottom center panel for $e = 0.2724 > e_{23}$; in this regime, the separatrix starting from the saddle equilibrium surrounds the center equilibrium in $\psi = \pi/2$; moreover, the rotational curves have a non-twist behavior (the same happens for Chariklo 1). In the bottom right panel, there are still the two equilibria in $\psi = \pi/2$, but a different regime appears: the separatrix does not surround the center equilibrium in $\psi = \pi/2$ and the non-twist rotational curves disappear. The behavior of the 2:3 resonance points out its dynamical instability.

For all three small bodies and sample cases, the smaller amplitude of libration around the 1:3 resonance, coupled with its extended stability duration with respect to the other resonances and the lack of bifurcations, provides a positive resolution to (Q1), since these elements show a marked robustness of the 1:3 resonance with respect to the 1:1, 1:2, 2:3 resonances. This result has been obtained by considering just the potential of the central body, thus providing a positive answer also to (Q2). Figure 2 shows that the amplitude of libration depends on the shape parameters. In connection to (Q3), we observe that the amplitude increases as jointly $\mathscr{E}$, Ω get larger, thus highlighting a different dynamical behavior between small bodies and planets.

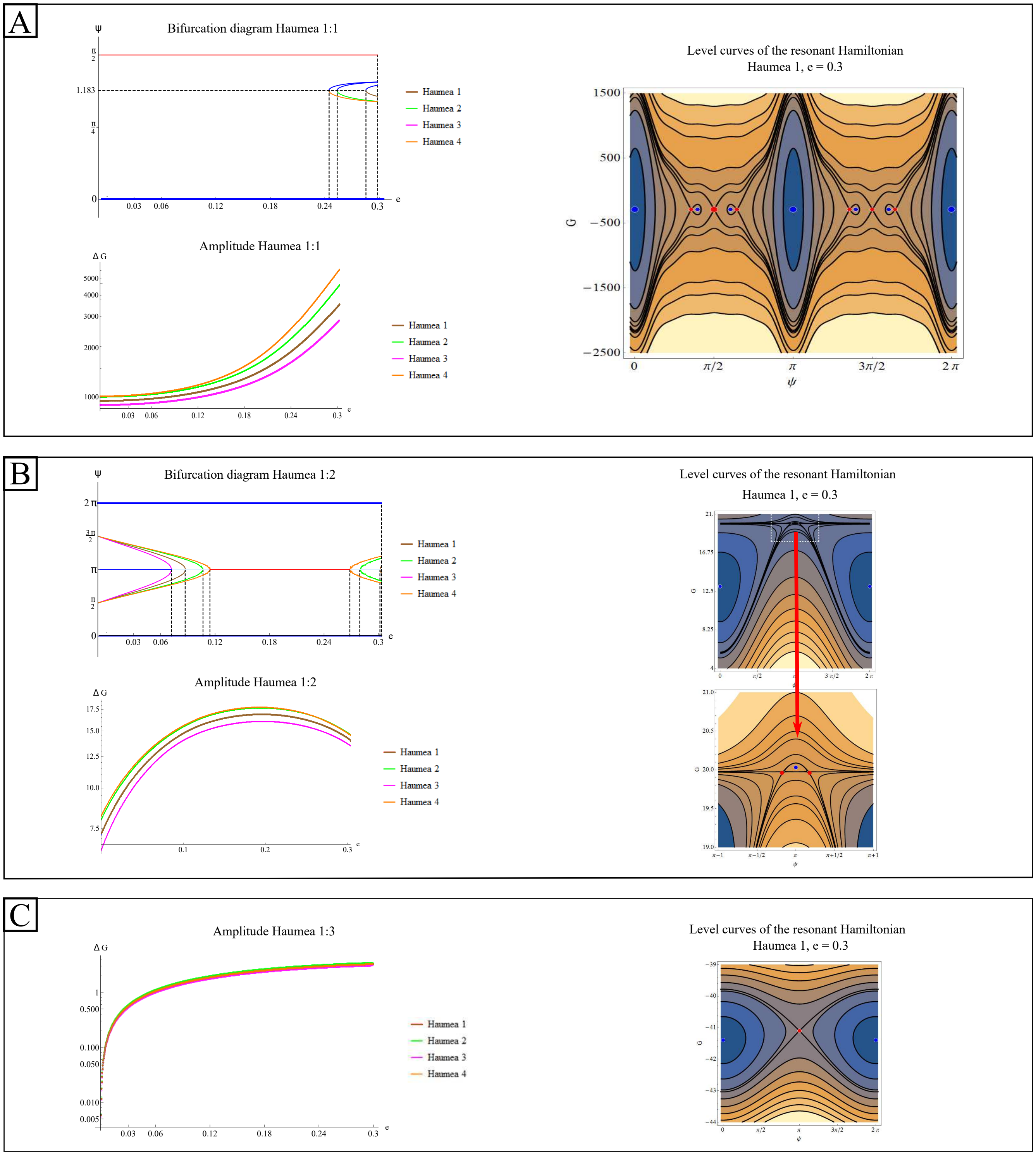

Figure 3. Haumea. Stability analysis for the 4 cases in Table 2, for the 1:1, 1:2 and 1:3 resonances. Panel A: 1:1 resonance; bifurcation diagram and amplitudes (left); phase portrait (right) of Haumea 1. Panel B: 1:2 resonance; bifurcation diagram and amplitudes (left); phase portrait (top right) of Haumea 1 (with a zoomed figure around $\psi = \pi$, bottom right). Panel C: 1:3 resonance; amplitudes (left; in this case, no bifurcations occur); phase portrait of Haumea 1 (right). In the bifurcation diagrams and the phase portraits, blue stands for center and red for saddle; in the bifurcation diagrams, coloured lines referred to the four cases stand for saddle.

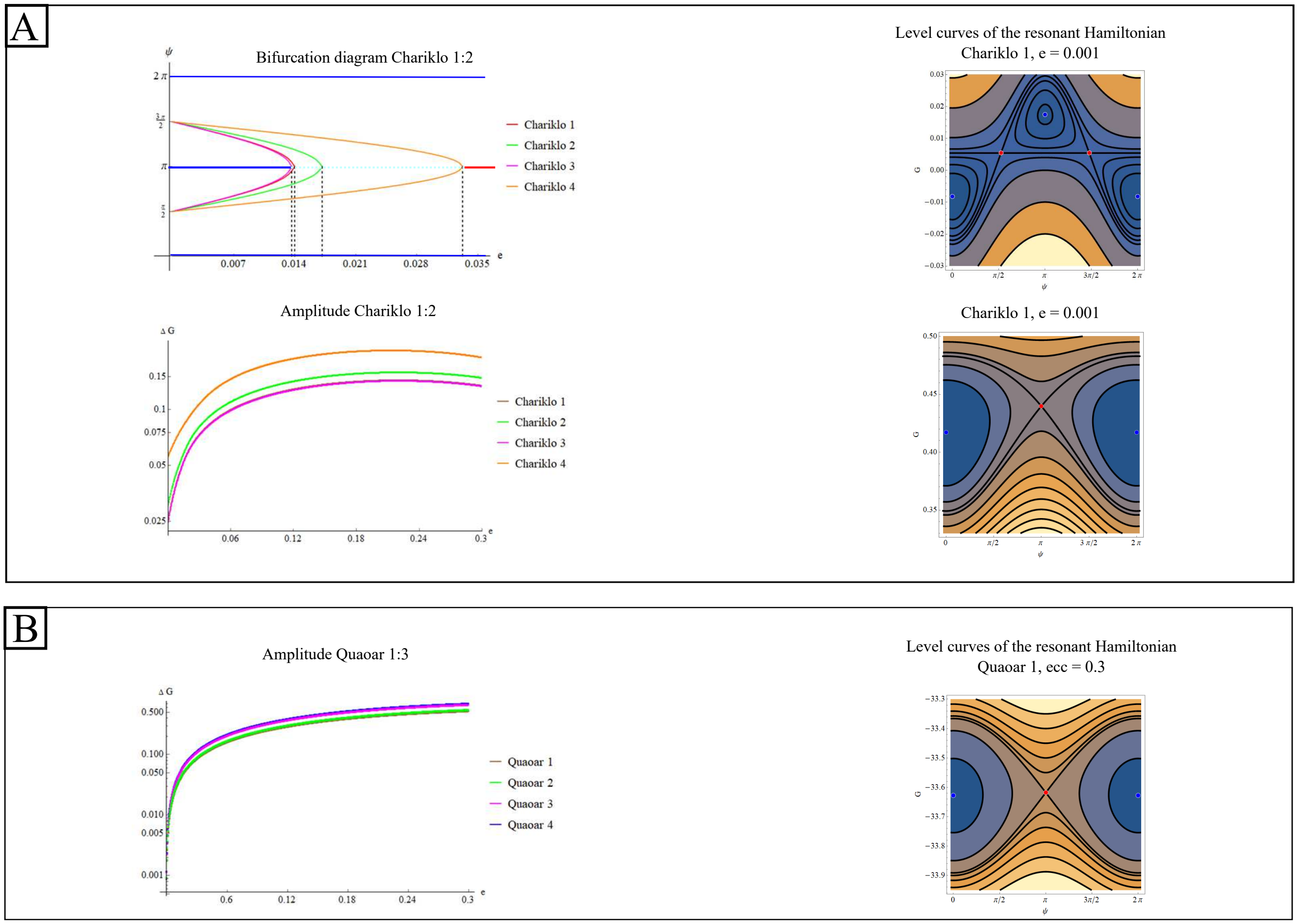

Figure 4. Chariklo and Quaoar for the four cases of Table 2. Panel A: Chariklo, 1:2 resonance; bifurcation diagram and amplitudes (left); phase portraits of Chariklo 1 at $e = 0.001$ and $e = 0.3$ (right). We recall that, in Chariklo, neither the corotation, nor the 1:3 resonance present bifurcation phenomena. Panel B: Quaoar, 1:3 resonance; amplitudes (left) and phase portrait for $e = 0.3$ for Quaoar 1 (right). In the bifurcation diagram and the phase portraits, blue stands for center and red for saddle; in the bifurcation diagram, coloured lines referred to the four cases stand for saddle.

3 Discussion

This study aims at examining the dynamical behavior of a set of resonances associated with particles that may be part of a ring system surrounding a small celestial body. The resonances were characterized by distinct features: the amplitude of libration around stable equilibria, the stability time for motions at resonance, the occurrence of bifurcations. These characteristics have been analyzed in terms of some parameters, precisely the eccentricity, elongation and oblateness[32–35]. Owing to the inherent uncertainties in determining certain physical parameters of Haumea, Chariklo and Quaoar, we have evaluated four representative scenarios for each celestial body. The findings suggest the establishment of a hierarchical framework among the resonances, wherein the 1:3 resonance emerges as the most probable outcome for all three bodies.

Our results are based on the triaxial ellipsoidal model which was selected due to its effective approximation for small bodies; the topographic feature model, frequently employed for Chariklo, was also evaluated and provides results similar to the ellipsoidal model[36]. A key assumption was that the ring's particle trajectory lies within the equatorial plane. We are aware that more sophisticated models might have been employed, such as incorporating multiple equatorial mass anomalies or considering orbits beyond the equatorial plane. However, we believe that the primary characteristics are effectively captured by the model including just the gravitational potential of the central body. A notable exception might occur when a satellite orbits the central object, since it may significantly affect the dynamics of ring particles, and its inclusion in the model is warranted. This scenario, which deserves further investigation, applies to Quaoar, which has a small satellite named Weywot.

Within the ellipsoidal model, the examination of the dynamics of rings surrounding celestial bodies was performed using epicyclic variables, which offer an appropriate tool to establish a precise definition of spin-orbit resonances and to introduce

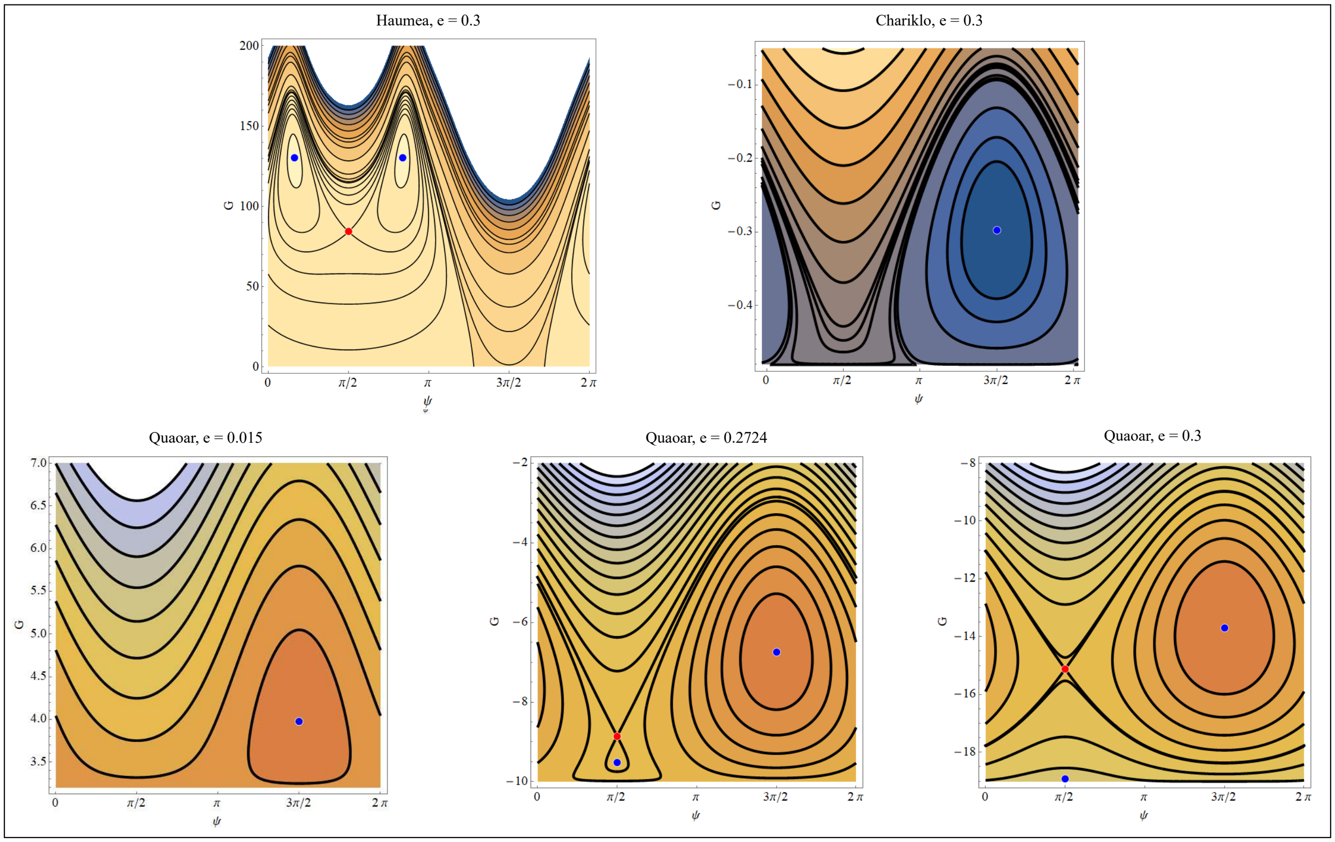

Figure 5. Phase portraits around the 2:3 resonance for Haumea 1 (top left panel), Chariklo 1 (top right panel) and Quaoar 1 (bottom panels) from Table 2. In all the panels, blue points stand for center equilibria and red points stand for saddle ones.

relevant action-angle variables. The non-axisymmetric component of the gravitational potential generates spin-orbit resonances, corresponding to commensurabilities between the rotational frequency of the small body and the orbital frequency of the ring's particle.

To analyze the dynamics of the resonances, we computed the libration amplitude surrounding the stable equilibria, we assessed the time of stability of the resonances using first-order estimates, and we examined the occurrence of bifurcations as a function of the eccentricity. In our investigation, we have taken into account the most significant terms in the series expansion of the gravitational potential, specifically with respect to the spherical harmonic coefficients. Incorporating additional terms can enhance the precision of the calculations; however, such refinement does not markedly influence the fundamental dynamical characteristics of the resonances.

The hierarchical selection of the resonances by small celestial bodies is substantiated by all analyzed dynamical features. The optimal conditions are invariably associated with the 1:3 resonance, which is characterized by the minimal amplitude of libration, the maximal stability time, and the lack of bifurcations.

It is essential to acknowledge that bifurcations have the potential to induce dynamical instability, as small variations in the initial conditions or parameters in proximity to the bifurcation points can substantially modify the dynamical behavior. Given the existence of critical eccentricity values at which bifurcations are observed, it is conceivable that the evolutionary trajectories of the orbital elements of small celestial bodies have undergone variations in eccentricity at intervals inducing bifurcation phenomena. Such variations in eccentricity might have originated from dissipative forces, potentially active during the early stages of the Solar system's formation. Should such variations in eccentricity determine bifurcations, it is plausible that the 1:3 resonance exhibited an increased likelihood of persistence compared to other resonances where bifurcations occurred with greater frequency. Additionally, it is important to acknowledge that an essential aspect is the location of the resonances in relation to the central body, particularly with regard to the Roche limit, as observed in previous studies[24]. In this respect, the 1:1 resonance, even if not displaying bifurcations, is always very close to the central body.

The conclusions of this work are applicable to significantly aspherical bodies characterized by high oblateness and elongation values; however, analogous behaviors concerning stability time and bifurcation occurrences have been identified even in nearly spherical models[37]. In this work, we have shown that the influence of substantial oblateness and elongation is relevant in determining the positions of the equilibria; moreover, we have found that the shape parameters considerably affect the libration amplitudes.

4 Methods

We provide details on the construction of the resonant Hamiltonian used in Sections 2 and 3 to analyze the local dynamics of a ring's particle around the 1:1, 1:2, 1:3, 2:3 resonances. We start with the derivation of the potential $V(r,\theta)$ generated by a rotating triaxial ellipsoid on a particle orbiting on its equatorial plane. Later, we introduce the epicyclic variables, particularly suited to treat the problem, and in this setting we construct the resonant Hamiltonians associated to the resonances under study.

Let us start by considering a triaxial ellipsoid, having axes $a > b > c > 0$ and rotating around the smallest axis with angular velocity Ω_P. Consider a fixed reference frame (O,x,y,z) with the $z-$axis coinciding with the spin axis and centered at the body's barycenter. Given a massless particle on the $xy-$plane, denote by r its distance from the origin and by L the true longitude, that is, the angle with respect to the $x-$axis. Let us introduce the time-dependent angle

$$\theta = L - \Omega_P t,$$

describing the relative position of the particle with respect to the rotating central body. The gravitational potential $V(r,\theta)$ generated by the ellipsoid on the particle can be expressed in terms of (r,θ) as an expansion in spherical harmonics[24]:

$$V(r,\theta) = -\frac{\mathscr{G}M_P}{r}\sum_{p=0}^{\infty}\cos(2p\theta)\sum_{l=p}^{\infty}\left(\frac{R}{r}\right)^{2l} C_{2l,2p}P_{2l,2p}(0),$$

where:

- $\mathscr{G}$ is the gravitational constant and M_p is the mass of the central body;
- the reference radius R has been introduced in (2);
- $C_{2l,2p}$ are suitable coefficients depending on $\mathscr{E}$ and Ω, as defined in Eq.(1), through a,b,c, with the following expression:

$$C_{2l,2p} = \frac{3}{R^{2l}}\frac{l!(2l-2p)!}{2^{2p}(2l+3)(2l+1)!}(2-\delta_{0,p})\sum_{k=0}^{\left[\frac{l-p}{2}\right]}\frac{(a^2-b^2)^{p+2k}\left(c^2-(a^2+b^2)/2\right)^{l-p-2k}}{16^k(l-p-2k)!(p+k)!k!}\ ,$$

  where $\delta_{0,p}$ is the Kronecker symbol;
- $P_{2l,2p}(0)$ are the Legendre polynomials computed in $x=0$, where

$$P_{i,j}(x) = (-1)^j\frac{(1-x^2)^{j/2}}{2^i i!}\frac{d^{i+j}}{dx^{i+j}}\left((x^2-1)^i\right).$$

Notice that the invariance with respect to a rotation of angle π on the equatorial plane implies that only even terms in the cosine of θ appear in the expansion of $V(r,\theta)$.
The Hamiltonian describing the particle's motion in a synodic reference frame, rotating with the central body, is

$$\mathscr{H}(p_r,p_\theta,r,\theta) = \frac{p_r^2}{2}+\frac{p_\theta^2}{2r^2}-\Omega_P p_\theta + V(r,\theta), \tag{8}$$

where p_r and p_θ are, respectively, the momenta of r and θ.
The potential $V(r,\theta)$ can be split as the sum of the axisymmetric part V_s, depending only on r, and the non-axisymmetric part, V_{ns}:

$$\begin{aligned}V(r,\theta) &= V_s(r)+V_{ns}(r,\theta)\\ &= -\frac{\mathscr{G}M_P}{r}\sum_{l=0}^{\infty}\left(\frac{R}{r}\right)^{2l}C_{2l,0}P_{2l,0}(0)-\frac{\mathscr{G}M_P}{r}\sum_{p=1}^{\infty}\cos(2p\theta)\sum_{p=1}^{l}\left(\frac{R}{r}\right)^{2l}C_{2l,2p}P_{2l,2p}(0)\ .\end{aligned}$$

The squares of the mean motion n and the epicyclic frequency κ can be expressed in term of $V_s(r)$ as

$$n^2(r) = \frac{1}{r}\frac{dV_s(r)}{dr},\quad \kappa^2(r) = \frac{3}{r}\frac{dV_s(r)}{dr}+\frac{d^2V_s(r)}{dr^2}.$$

Recalling that the synodic frequency ν is defined as $\nu = n - \Omega_P$, one can introduce the Lindblad resonance of order $m:(m-j)$ (with m, j integers) as in Eq. (3).

To study the local dynamics of the particle close to a resonance, let us fix $m, j \in \mathbb{Z}$ and consider r_* as the resonant radius associated to the resonance $m:(m-j)$, which is the solution of the equation

$$j\kappa(r_*) = m\left(n(r_*) - \Omega_P\right).$$

We introduce the values n_*, κ_* as $n_* = n(r_*)$, $\kappa_* = \kappa(r_*)$. Locally around r_*, we consider the variables ρ, p_ρ, I, defined as

$$\rho = r - r_*,\ p_\rho = p_r,\ I = p_\theta - n_* r_*^2\,.$$

Expanding (8) around $\rho = 0$ and considering the symplectic change of coordinates $(\rho, p_\rho) \mapsto (\varphi, J)$ defined by

$$\rho = \sqrt{\frac{2J}{|\kappa_*|}}\sin\varphi, \quad p_\rho = \sqrt{2|\kappa_*|J}\cos\varphi, \tag{9}$$

the Hamiltonian (8) takes the form

$$\mathscr{H}(J,I,\varphi,\theta) = |\kappa_*|J + \nu_* I + \sum_{|i|=0}^{\infty}\sum_{j=0}^{\infty}\left(a_{2i,j}\cos(2i\theta + j\varphi) + b_{2i,j}\sin(2i\theta + j\varphi)\right), \tag{10}$$

where $\nu_* = n_* - \Omega_P$. The action-angle coordinates (J, I, φ, θ) are called *epicyclic* variables; the Hamiltonian (10) can be split taking separately the terms coming from the expansion of $V_s(r)$ and those coming from $V_{ns}(r,\theta)$:

$$\mathscr{H}(J,I,\varphi,\theta) = |\kappa_*|J + \nu_* I + F_s(J,I,\varphi) + F_{ns}(J,\varphi,\theta)\,,$$

where F_s and F_{ns} can be expanded as

$$\begin{aligned} F_s(J,I,\varphi) &= -2\frac{n_*}{r_*}I\sqrt{\frac{2J}{|\kappa_*|}}\sin\varphi + \frac{I^2}{2r_*^2} + \sum_{i=0}^{2}\sum_{j=3-i}^{\infty} d_{i,j} I^i J^{j/2}\sin^j\varphi, \\ F_{ns}(J,\varphi,\theta) &= \sum_{j=0}^{\infty}\sum_{i=1}^{\infty} V_{j,i} J^{j/2}\cos 2i\theta \sin^j\varphi \end{aligned}$$

with $d_{i,j}$ and $V_{j,i}$ being suitable coefficients, which can be computed explicitly.

In the actual computations, the sum (10) is truncated up to order 5, meaning up to the 10-th harmonic in θ and up to order 16 in ρ (corresponding to order 8 in J).

The resonant angle of order $m:(m-j)$ is given by $\psi = -m\theta + j\varphi$. To study the dynamics around a specific resonance, we consider the *resonant Hamiltonian*, taking only the terms of (10) which depend only on the actions (the *secular* ones) and those depending on the actions and the sole resonant angle (the *resonant* terms). At this stage, it is then possible to introduce a linear change of coordinates $(J, I, \varphi, \theta) \mapsto (G, L, \psi, \mu)$, where the angle μ is cyclic and thus $L = L_0$ is a constant of the motion fixed by the initial conditions.

Table 3 shows the coefficients (m, j), the resonant angle and the linear transformations used to construct the resonant Hamiltonians corresponding the cases 1:1, 1:2, 1:3 and 2:3. Notice that, given that the angle θ appears only with even multiples, the value m is always an even integer.

One then arrives at the 1D resonant Hamiltonian as written in (4):

$$\mathscr{H}(G,\psi;L_0) = \alpha_1(L_0)G + \alpha_2(L_0)G^2 + \beta_1(G;L_0)\ \mathrm{cs}(\psi) + \beta_2(G;L_0)\ \mathrm{cs}(2\psi)\,, \tag{11}$$

where L_0 is a fixed parameter and where, according to the chosen resonance, cs stands for cosine or sine and α_i, β_i are polynomials. To choose a value of L_0, we first determine initial values of J and I, say J_0 and I_0, and then use the transformations in Table 3 to compute L_0. As for the value of J_0, we use (9) to get

$$J_0 = \frac{p_\rho^2}{2|\kappa_*|} + \frac{|\kappa_*|\rho^2}{2},$$

choosing, according to Kepler's relations, $\rho = er_*$, $p_\rho = r_* n_* e$, where e is the eccentricity of the particle's orbit. On the other hand, one can fix the initial value of I_0 as

$$I_0 = n(r_* + er_*)\,(r_* + er_*)^2 - n_* r_*^2.$$

Once obtained the 1D Hamiltonian (11), one can proceed to the local analysis of the resonances.

Resonance	(m,j)	Resonant angle	Linear change of coordinates
1:1	$(-2,0)$	$\psi=\theta$	$\begin{cases}G=I,\ \psi=2\theta\end{cases}$
1:2	$(-2,2)$	$\psi=2\theta+2\phi$	$\begin{cases}G=-J/2+I,\ \psi=2\theta+2\phi\\ L=J-I,\ \mu=\theta+2\phi\end{cases}$
1:3	$(-2,4)$	$\psi=2\theta+4\phi$	$\begin{cases}G=(J-I)/2,\ \psi=2\theta+4\phi\\ L=-J+2I,\ \mu=\theta+\phi\end{cases}$
2:3	$(-2,1)$	$\psi=2\theta+\phi$	$\begin{cases}G=-J+I,\ \psi=2\theta+\phi\\ L=J-I/2,\ \mu=2(\theta+\phi)\end{cases}$

Table 3. Resonances considered in the paper with the corresponding coefficients (m,j), the associated resonant angle and the linear change of variables $(J,I,\varphi,\theta)\mapsto(G,L,\psi,\mu)$ to construct the corresponding resonant Hamiltonian.

References

1. Ortiz, J. L. *et al.* The size, shape, density and ring of the dwarf planet Haumea from a stellar occultation. *Nature* **550**, 219–223, DOI: 10.1038/nature24051 (2017). 2006.03113.
2. Marzari, F. Ring dynamics around an oblate body with an inclined satellite: the case of Haumea. *Astron. & Astroph.* **643**, A67, DOI: 10.1051/0004-6361/202038812 (2020). 2008.13415.
3. Winter, O. C., Borderes-Motta, G. & Ribeiro, T. On the location of the ring around the dwarf planet Haumea. *MNRAS* **484**, 3765–3771, DOI: 10.1093/mnras/stz246 (2019). 1902.03363.
4. Braga-Ribas, F. *et al.* A ring system detected around the Centaur (10199) Chariklo. *Nature* **508**, 72–75, DOI: 10.1038/nature13155 (2014). 1409.7259.
5. Giuliatti Winter, S. M. *et al.* The stability around Chariklo and the confinement of its rings. *Astron. & Astroph.* **679**, A62 (2023).
6. Gomes-Junior, A. R., Mitidiero, A. L. R., Morgado, B. E. & Sicardy, B. Characterizing longitude variation on Chariklo's main ring. *Philos. Transactions Royal Soc. A: Math. Phys. Eng. Sci.* **383**, 20240199, DOI: 10.1098/rsta.2024.0199 (2025).
7. Morgado, B. E. *et al.* Refined physical parameters for Chariklo's body and rings from stellar occultations observed between 2013 and 2020. *Astron. & Astroph.* **652**, A141, DOI: 10.1051/0004-6361/202141543 (2021).
8. Hedman, M. M. A planetary ring in a surprising place. *Nature* **614**, 232–233, DOI: 10.1038/d41586-023-00270-3 (2023).
9. Morgado, B. E. *et al.* A dense ring of the trans-Neptunian object Quaoar outside its Roche limit. *Nature* **614**, 239–243, DOI: 10.1038/s41586-022-05629-6 (2023).
10. Pereira, C. L. *et al.* The two rings of (50000) Quaoar. *Astron & Astroph.* **673**, L4, DOI: 10.1051/0004-6361/202346365 (2023). 2304.09237.
11. Sicardy, B., Braga-Ribas, F., Buie, M. W., Ortiz, J. & Roques, F. Stellar occultations by trans-neptunian objects. *The Astron. Astrophys. Rev.* **32**, 6, DOI: 10.1007/s00159-024-00156-x (2024).
12. Murray, C. D. & Dermott, S. F. Solar System Dynamics. *Camb. Univ. Press.* (1999).
13. Borderies, N. & Longaretti, P. Y. Description and behavior of streamlines in planetary rings. *Icarus* **72**, 593–603, DOI: 10.1016/0019-1035(87)90055-8 (1987).
14. Celletti, A., De Blasi, I. & Di Ruzza, S. Perturbative methods and synchronous resonances in Celestial Mechanics. *Appl. Math. Model.* **143** (2025).
15. Goldreich, P. & Tremaine, S. The dynamics of planetary rings. *Ann. Rev. Astron. Astroph.* **20**, 249–283, DOI: 10.1146/annurev.aa.20.090182.001341 (1982).

16. Murray, C. D. Planetary Ring Dynamics. *Philos. Transactions Royal Soc. Lond. Ser. A* **349**, 335–344, DOI: 10.1098/rsta.1994.0136 (1994).

17. Sicardy, B. Dynamics of Planetary Rings. In Souchay, J. (ed.) *Dynamics of Extended Celestial Bodies and Rings*, vol. 682, 183, DOI: 10.1007/3-540-32455-0_9 (2006).

18. Sicardy, B. Resonances in Nonaxisymmetric Gravitational Potentials. *Astron. J.* **159**, 102, DOI: 10.3847/1538-3881/ab6d06 (2020). 2001.06382.

19. Tiscareno, M. S. Planetary Rings. In Oswalt, T. D., French, L. M. & Kalas, P. (eds.) *Planets, Stars and Stellar Systems. Volume 3: Solar and Stellar Planetary Systems*, 309, DOI: 10.1007/978-94-007-5606-9_7 (2013).

20. Balmino, G. Gravitational Potential Harmonics from the Shape of an Homogeneous Body. *Celest. Mech. Dyn. Astron.* **60**, 331–364, DOI: 10.1007/BF00691901 (1994).

21. Boyce, W. Comment on a Formula for the Gravitational Harmonic Coefficients of a Triaxial Ellipsoid. *Celest. Mech. Dyn. Astron.* **67**, 107–110, DOI: 10.1023/A:1008224825003 (1997).

22. Ribeiro, T., Winter, O. C., Madeira, G. & Giuliatti Winter, S. M. Dynamics around non-spherical symmetric bodies: II. The case of a prolate body. *MNRAS* **525**, 44–56, DOI: 10.1093/mnras/stad2362 (2023).

23. Madeira, G., Giuliatti Winter, S. M., Ribeiro, T. & Winter, O. C. Dynamics around non-spherical symmetric bodies - I. The case of a spherical body with mass anomaly. *MNRAS* **510**, 1450–1469, DOI: 10.1093/mnras/stab3552 (2022). 2112.01817.

24. Sicardy, B. *et al.* Ring dynamics around non-axisymmetric bodies with application to Chariklo and Haumea. *Nat. Astron.* **3**, 146–153, DOI: 10.1038/s41550-018-0616-8 (2019). 1811.09437.

25. Leiva, R. *et al.* Size and shape of Chariklo from multi-epoch stellar occultations. *Astron. J.* **154**, 159, DOI: 10.3847/1538-3881/aa8956 (2017).

26. Kiss, C. *et al.* The visible and thermal light curve of the large Kuiper belt object (50000) Quaoar. *Astron. & Astroph.* **684**, A50, DOI: 10.1051/0004-6361/202348054 (2024).

27. Melita, M. D., Duffard, R., Ortiz, J. L. & Campo-Bagatin, A. Assessment of different formation scenarios for the ring system of (10199) Chariklo. *Astron. & Astroph.* **602**, A27, DOI: 10.1051/0004-6361/201629858 (2017).

28. Celletti, A. *Stability and Chaos in Celestial Mechanics* (Springer-Verlag, Berlin; published in association with Praxis Publishing, Chichester, 2010).

29. De Blasi, I., Celletti, A. & Efthymiopoulos, C. Semi-Analytical Estimates for the Orbital Stability of Earth's Satellites. *J. NonLinear Sci.* **31**, 93, DOI: 10.1007/s00332-021-09738-w (2021). 2101.05340.

30. Celletti, A., De Blasi, I. & Efthymiopoulos, C. Nekhoroshev estimates for the orbital stability of Earth's satellites. *Celest. Mech. Dyn. Astron.* **135**, 10, DOI: 10.1007/s10569-023-10124-9 (2023).

31. Pöschel, J. Nekhoroshev estimates for quasi-convex hamiltonian systems. *Math. Zeitschrift* **213**, 187–216, DOI: 10.1007/BF03025718 (1993).

32. Belbruno, E., Gidea, M. & Lam, W.-T. Regularization of the Hill four-body problem with oblate bodies. *Celest. Mech. Dyn. Astron.* **135**, 6, DOI: 10.1007/s10569-023-10122-x (2023). 2209.13625.

33. Brown, G. M. & Scheeres, D. J. Analyzing the structure of periodic orbit families that exist around asteroid (101955) Bennu. *Celest. Mech. Dyn. Astron.* **135**, 52, DOI: 10.1007/s10569-023-10164-1 (2023).

34. Fu, X., Soldini, S., Ikeda, H., Scheeres, D. J. & Tsuda, Y. The dynamics about asteroid (162173) Ryugu. *Celest. Mech. Dyn. Astron.* **136**, 29, DOI: 10.1007/s10569-024-10199-y (2024).

35. Rosaev, A. Resonance perturbation of (5026) Martes and 2005 WW113 asteroid pair. *Celest. Mech. Dyn. Astron.* **136**, 41, DOI: 10.1007/s10569-024-10209-z (2024).

36. Celletti, A., De Blasi, I. & Di Ruzza, S. Stability analysis of resonances around small bodies with a topographic feature. *Preprint* (2025).

37. Celletti, A., De Blasi, I. & Di Ruzza, S. Stability and bifurcations of resonances in ring's dynamics. *Preprint* (2025).

Funding

I.D.B. is supported by the Italian Research Center on High Performance Computing Big Data and Quantum Computing (ICSC), project funded by European Union - NextGenerationE and National Recovery and Resilience Plan (NRRP) - Mission 4 Component 2. Spoke 3, Astrophysics and Cosmos Observations.
I.D.B. and S.D.R. are partially supported, respectively, by INdAM groups G.N.A.M.P.A and G.N.F.M.

Author contributions statement

Alessandra Celletti, Irene De Blasi, Sara Di Ruzza contributed equally to all phases of preparation of the article; they all conceived the research, elaborated the analytical methods and the programs, wrote the manuscript.

Additional information

Accession codes: the codes used in this paper are available upon reasonable request.
Competing interests: The authors declare no competing interests.